Ecotoxicology and Environmental Safety 208 (2021) 111543

Contents lists available at ScienceDirect

Ecotoxicology and Environmental Safety

journal homepage: www.elsevier.com/locate/ecoenv

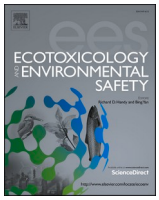

Research Paper

Acrylamide inhibits autophagy, induces apoptosis and alters cellular metabolic profiles

Dan Song [a,d], Chao Xu [a], Askild L. Holck [e], Rong Liu [a,b,c,*]

[a] College of Food Science and Technology, Nanjing Agricultural University, Nanjing, China
[b] National center for international research on animal gut nutrition, Nanjing, China
[c] Jiangsu collaborative innovation center of meat production and processing, Nanjing, China
[d] College of Animal Science and Technology, Zhejiang Agriculture and Forestry University, Hangzhou, China
[e] Norwegian Institute of Food, Fisheries and Aquaculture Research (NOFIMA), P.O. Box 210, N-1431 Aas, Norway

ARTICLE INFO

Edited by: Dr. Caterina Faggio

Keywords:
Acrylamide
Metabolomics
Autophagy
Apoptosis
Inflammation

ABSTRACT

Acrylamide (ACR) is generated during thermal processing of carbohydrate-rich foods at high temperature and can directly enter the body through ingestion, inhalation and skin contact. The toxicity of ACR has been widely studied. The main results of these studies show that exposure to ACR can cause neurotoxicity in both animals and humans, and show reproductive toxicity and carcinogenicity in rodent animal models. However, the mechanism of toxicity of ACR has not been studied by metabolomics approaches, and the effect of ACR on autophagy remains unknown. Here, U_2OS cell were treated with ACR 6 and 24 h and collected for further study. We have demonstrated that ACR inhibited autophagic flux, and increased ROS content. Accumulation of ROS resulted in increase of apoptosis rates and secretion of inflammatory factors. In addition, significant differences in metabolic profiles were observed between ACR treated and control cells according to multiple analysis models. A total of 73 key differential metabolites were identified. They were involved in multiple metabolic pathways. Among them, exposure to ACR caused glycolysis/gluconeogenesis attenuation by decreasing levels of glycolytic intermediates, reduced the rate of the TCA cycle, while elevating levels of several amino acid metabolites and lipid metabolites. In summary, our study provides useful evidence of cytotoxicity caused by ACR via metabolomics and multiple bioanalytic methods.

1. Introduction

Acrylamide (ACR) is a water-soluble white crystal chemical used in the production of polyacrylamide or acrylamide polymers, and is applied extensively in chemical industry for plastic processes (Exon, 2006; Friedman, 2003). It is generated during thermal processing of carbohydrate-rich foods such as potatoes or root vegetables at high temperatures (higher than 120 °C) through the Maillard reaction. The content of ACR depends on multiple factors, including food ingredients, processing conditions, such as temperature and time of cooking (Daniali et al., 2018; Vainio et al., 1994). In 1994, the International Agency for Research on Cancer (IARC) reported that ACR was classified as a substance of the Group 2A, i.e. as a probable human carcinogen and neurotoxin (Vainio et al., 1994). It is mainly based on the fact that ACR is a hydrophilic molecule and can directly enter the body through ingestion, inhalation and skin contact (Sumner et al., 2003) and is then metabolized into glycidamide, a carcinogenic active metabolite that combines with DNA strands, thereby causing neurotoxicity, genotoxicity and reproductive toxicity in several animal species and humans (Cheng et al., 2019; Kacar et al., 2019; Shipp et al., 2006; Tan et al., 2018). Moreover, increasing evidence has revealed that ACR is a soft electrophile, it creates ROS overproduction through the interaction with any proteins containing-SH and NH_2 groups to induce oxidative stress, and further damages DNA strands (Kacar et al., 2019). The damage to DNA strands resulting in multiple intracellular reactions and cancer in mammals, are the principal endogenous toxicity pathways in the biological system (Scharer, 2003; Taira et al., 2004). The relationship between dietary acrylamide intake and several common disease risks has received much attention recently. It has been reported that ACR causes mitochondrial dysfunction by decreasing expression of the mitochondrial complex I, III, and IV subunits and mitochondrial reserve capacity in BV-2 microglial cells (Liu et al., 2015), increases inflammatory

* Correspondence to: College of Food Science and Technology, Nanjing Agricultural University, Nanjing 210095, China.
E-mail address: liurong010@njau.edu.cn (R. Liu).

https://doi.org/10.1016/j.ecoenv.2020.111543
Received 3 August 2020; Received in revised form 15 October 2020; Accepted 19 October 2020

cytokine levels (NO, TNF-α, iNOS, nNOS, and COX-2) in zebrafish larvae (Krishnan and Kang, 2019), and induces nerve terminal degeneration, which is one of the characteristics of ACR-induced neurodegeneration (LoPachin et al., 2003).

Autophagy is a conserved lysosomal degradation process. Studies have shown that autophagy is able to reduce ROS production by promoting the degradation of misfolded proteins, lipids and damaged organelles. It plays crucial role in maintaining cellular homeostasis and in metabolic disorders (Delbridge et al., 2017; Galluzzi et al., 2017). In the process of autophagy, phospholipids play pivotal roles in initiation and phagophore formation, elongation and maturation, fusion and reformation of autolysosomes (Hsu and Shi, 2017; Mizushima and Levine, 2010). Our previous study has suggested that defective autophagy may cause lipid accumulation (Song et al., 2019b). Other research has demonstrated that ACR induced the mitochondrial-mediated apoptosis, and caused increased levels of LC3 in neuronal cells (Song et al., 2017). Tan et al. (2018) found that exposure to ACR significantly elevated the number of autophagy structures, and increased mRNA levels of autophagy-related genes, thereby causing excessive autophagy in the mouse hippocampus. However, the exact effect of ACR on autophagy still remains unclear, and the molecular mechanisms underlying ACR-mediated autophagy are not well understood.

The emergence and development of systems biology has brought a series of innovative technologies to quantify biomolecules at different levels and analyze the complex interaction between biomolecules. Metabolomics, an important part of systems biology, has been widely applied in many fields, such as disease diagnostics, toxicology, etc. It is a process of identifying and quantifying thousands of metabolites in a given sample, to elucidate the changes of endogenous metabolites, and better understand the chemical-induced toxicity. Metabolomics is a truly interdisciplinary field that combines analytical chemistry and multiple analytical platform technologies. Several analytical techniques have been used for investigations of metabolites, such as nuclear magnetic resonance (NMR) and multiple mass spectrometry separation techniques including gas-chromatography-mass spectrometry (GC-MS), liquid chromatography mass spectrometry (LC-MS), and Fourier transform mass spectrometry (FT-MS). High-resolution LC-MS represents the forefront of metabolomics technology, and liquid chromatography-quadrupole-orbitrap mass spectrometry (LC-Q-Orbitrap/MS) is a fragment ion scanning technology with extremely high resolution, sensitivity and mass accuracy (Zhang et al., 2017). It has been successfully used for metabolomics and lipomics analysis in complex matrices (animal tissues, plasma, cells, and agricultural products). Although the underlying molecular mechanisms of ACR toxicity have attracted considerable interest of researchers, little research has been done on the metabolomics profiling of ACR exposure. In this study, we investigated the effect of ACR on autophagy and compared the metabolic differences between ACR treated and control group using Q ExactiveOrbitrap mass spectrometer and determined key differential metabolites in combination with multivariate analysis. We demonstrate that ACR inhibits autophagy via blocking autophagic flux, and induces ROS generation, cell apoptosis as well as inflammation. Moreover, metabolomics results show that ACR exposure exhibits distinct metabolomic profiles different from those of the control, and alters multiple metabolic pathways. Our study contributes to provide useful cytotoxicity evidence of ACR exposure.

2. Material and methods

2.1. Reagents and antibodies

ACR (≥99%), chromatographic grades of methanol, autophagy activator Torin2 (SML1224), and autophagy inhibitor Chloroquine (CQ, C6628), mouse anti-β-tubulin (T8328), rabbit anti-LC3 (l7543) antibodies were procured from Sigma-Aldrich (St. Louis, MO, USA). Rabbit anti-p62 (ab109012) antibody was purchased from Abcam (Cambridge, UK). IgG-HRP (horse radish peroxidase) linked secondary antibodies were obtained from Sangon Biotech (Shanghai, China). ACR was dissolved in sterilized deionized water to obtain a stock solution of 1 M and stored at − 20 °C, and then diluted to the desired concentration.

2.2. Western blotting

Cell protein samples were collected, denatured, and separated by sodium dodecyl sulfate polyacrylamide gel electrophoresis (SDS-PAGE). Subsequently, proteins were transferred to polyvinylidene fluoride (PVDF) membranes (Biorad, Hercules, USA), and incubated with corresponding primary and HRP conjugated secondary antibodies. Thereafter, the membrane was washed in PBST buffer three times and the protein bands were detected by chemiluminescence with an imaging system, and then analyzed using Image J software.

2.3. Flow cytometry

Apoptosis was evaluated by flow cytometry with Annexin V/FITC-PI kit (Vazyme, A211) according to instructions by the producer. Cells were treated with 10 μM ACR for 24 h before being collected and re-suspended in 100 μL binding buffer, and stained with 5 μL of Annexin V-FITC and 5 μL of propidium iodide (PI) together for 10 min at room temperature in the dark. Thereafter, 400 μL additional binding buffer was added to the cells, and then the rate of apoptosis were measured by a BD Accuri C6 flow cytometer.

2.4. ROS detection

The production of ROS was assessed with a DCFH-DA (2′,7′-dichlorodihydrofluorescein diacetate) based assay. DCFH-DA is a cell-permeable non-fluorescent probe. It is de-esterified intracellularly and turns into highly fluorescent 2′,7′-dichlorofluorescein upon oxidation by ROS. U_2OS cells were cultured on Lab-Tek Chambered Coverglass units and treated with 10 μM ACR for 24 h. Then cells were incubated with 10 μM DCFH-DA at 37 °C for 30 min in the dark and observed under a laser scanning confocal microscopy (Olympus FV1300).

2.5. RNA extraction and quantitative real-time PCR

Quantitative real-time PCR was performed as described previously (Song et al., 2019b). Briefly, total RNA was extracted from U_2OS cells using TRIzol reagent (TransGen Biotech). PrimeScript II First Strand cDNA Synthesis Kit (TaKaRa, Dalian), a commercial kit, was specifically used for cDNA synthesis (Tai et al., 2015), and gene expression analysis was performed by PCR on a CFX 96 real-time PCR system instrument (Bio-Rad, USA). Gene expressions were normalized against GAPDH. All samples were run in triplicate. Primer sequences are shown in Table S1.

2.6. Metabolite extraction

U_2OS cells, following treatment with 10 μM ACR for 6 h, were washed with cold Phosphate Buffered Saline (PBS) three times gently, added 2 mL 80% (v/v) methanol (pre-chilled to −80 °C), and then incubated at − 80 °C for 1 h. Cells were collected and centrifuged at 14,000 g for 20 min at 4 °C. Subsequently, the supernatant was collected in another clean tube and dried using nitrogen. The dried samples were stored in dry ice for subsequent analysis.

2.7. Metabolite profiling analysis

Non-targeted metabolomics analysis was performed using a Q ExactiveOrbitrap mass spectrometer (Thermo, CA). One μL of supernatant was added to the chromatography columns. Atlantis HILIC Silica columns were used in positive mode and BEH Amide columns were used for LC separation in negative mode. Bound metabolites were eluted with

a gradient of solvent A (containing 5 mM ammonium acetate, pH 9.0) using 1–99% solvent B (95% acetonitrile with 5 mM ammonium acetate, pH 9.0) within 15 min. Buffer was adjusted to pH 9.0 with ammonium hydroxide. Data with mass ranges of *m/z* 70–1,050 were acquired at positive ion mode and *m/z* 80–1,200 at negative mode. The full mass spectrometry (MS) resolution was 70,000 and MS/MS resolution was 17,500. The source parameters were as follows: spray voltage: 3.0 kV; capillary temperature: 320 °C; heater temperature: 300 °C; sheath gas flow rate (arb): 35; auxiliary gas flow rate: 10; duty cycle, 1.2 s. For metabolites analysis, reliable metabolite screening, identification, and confirmation were based on Tracefinder 3.2 software (Thermo Fisher Scientific) (Li et al., 2016a) searches with a home-built database, with a MS1 mass error of < 8 ppm and MS2 mass error of < 15 ppm. Quality control (QC) samples were analyzed to assess the stability of the detection system and quality of data.

2.8. Data processing and statistical analysis

The obtained raw data was analyzed using Tracefinder 3.2 (Thermo Fisher Scientific) based on two levels of identification, including accurate mass matching and MS/MS confirmation. After peak extraction, alignment, integration and normalization, statistical analysis was conducted with the MetaboAnalyst software for multivariate analysis. Firstly, the unsupervised principal component analysis (PCA) was employed to observe distribution between ACR and control groups. Secondly, partial least squares-discriminant analysis (PLS-DA) score plot, a supervised analysis, was performed to further discriminate the classification and identify potential biomarkers. Two hundred times random permutation tests were conducted to validate the reliability of the PLS-DA model. Subsequently, hierarchical clustering analysis was carried out using MetaboAnalyst and pathways were analyzed with Metabolomics Pathway Analysis (MetPA) based on the kyoto encyclopedia of genes and genomes (KEGG) Pathway Database (Available online: http://www.genome.jp/kegg).

Quantitative data were expressed as means±SEM and analyzed from at least three separate experiments by one-way ANOVA or two-tailed Student's *t*-test depending on specific experiments. The statistical significance of difference was set as $P < 0.05$.

3. Results

3.1. ACR induces the accumulation of autophagic vacuoles

In order to determine the effect of ACR on autophagy, we treated the U_2OS cell with different concentrations of ACR for 6 h. Torin2 (50 nM) and CQ (2 μM) served as controls promoting and inhibiting autophagy, respectively (the same below). LC3 is an important autophagy protein involved autophagosome formation. We detected the level of LC3-II by western blotting. This result showed that ACR treatment from 10 nM to 10 μM significantly increased LC3-II levels (Fig. 1A, B). Then, we treated U_2OS cell with ACR at a dose of 1 μM for different hours. Signals were normalized against those of β-tubulin. LC3-II levels were significantly increased in a time-dependent manner from 1 to 6 h (Fig. 1C, D). Taken together, these results indicate that ACR induces autophagic vacuoles accumulation.

3.2. ACR blocks autophagic degradation

It was reported that the accumulation of autophagic vacuoles could be due to the accelerated autophagosome formation or the blocked autophagy degradation (Song et al., 2019b). p62 is an important autophagy protein, which is degraded during the fusion process of autophagosome and lysosome. The levels of p62 were significantly increased when cells were treated with from 10 nM to 10 μM ACR. This result was consistent with increased LC3-II levels (Fig. 2A, B), and ACR significantly elevated p62 levels from 3 h to 6 h (Fig. 2C, D). It was obvious that, ACR treatment significantly increased p62 levels in a dose- and time-dependent manner. These results indicate that ACR inhibits autophagic degradation.

3.3. ACR blocks autophagy flux

The above results showed that exposure to ACR caused LC3-II and p62 levels accumulation, and this effect was similar to CQ. Thus we hypothesized that ACR may block autophagic flux. Subsequently, an autophagy flux assay was performed to further examine this assumption. We treated U_2OS cells with different treatments as shown in Fig. 3. We

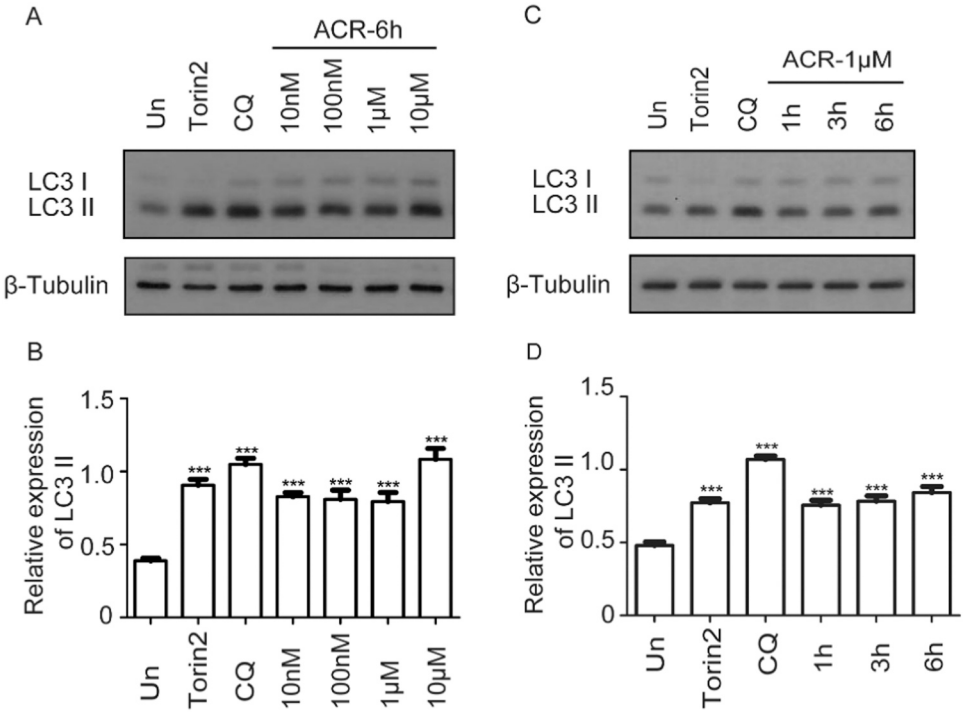

Fig. 1. ACR treatment induces LC3-II accumulation in U_2OS cells. (A) U_2OS cells were treated with different concentration of ACR for 6 h. LC3-II levels were detected by western blotting. (B) Statistical analysis of LC3-II from triplicate experiments in A. (C) U_2OS cells were treated with ACR at 1 μM for different times and level of LC3-II was examined by western blotting. (D) Statistical analysis of LC3-II from triplicate experiments in C. Data are shown as the mean ± SEM and analyzed by one-way ANOVA with Dunnett's multiple comparisons test. $^*P < 0.05$, $^{**}P < 0.01$, $^{***}P < 0.001$. Un: untreated controls.

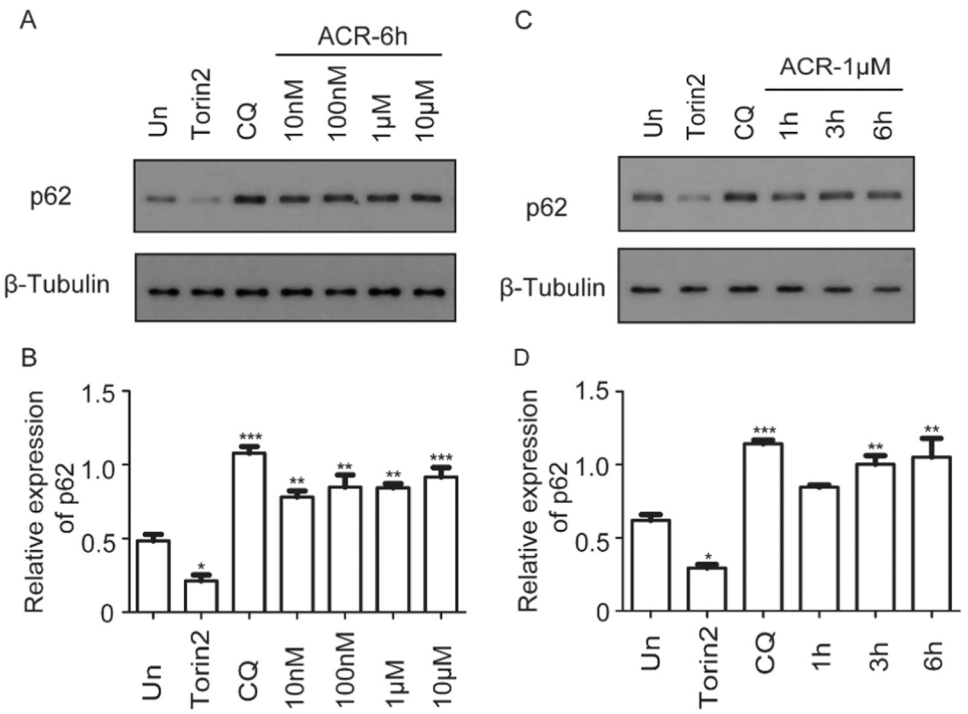

Fig. 2. ACR treatment inhibits autophagic degradation in U_2OS cells. (A) U_2OS cells were treated with different concentrations of ACR for 6 h. p62 levels were detected by western blotting. (B) Statistical analysis of p62 from triplicate experiments in A. (C) U_2OS cells were treated with ACR at a dose of 1 μM for different times and the levels of p62 were examined by western blotting. (D) Statistical analysis of p62 from triplicate experiments in C. Data are shown as the mean ± SEM and analyzed by one-way ANOVA with Dunnett's multiple comparisons test. $^{*}P < 0.05$, $^{**}P < 0.01$, $^{***}P < 0.001$. Un: untreated controls.

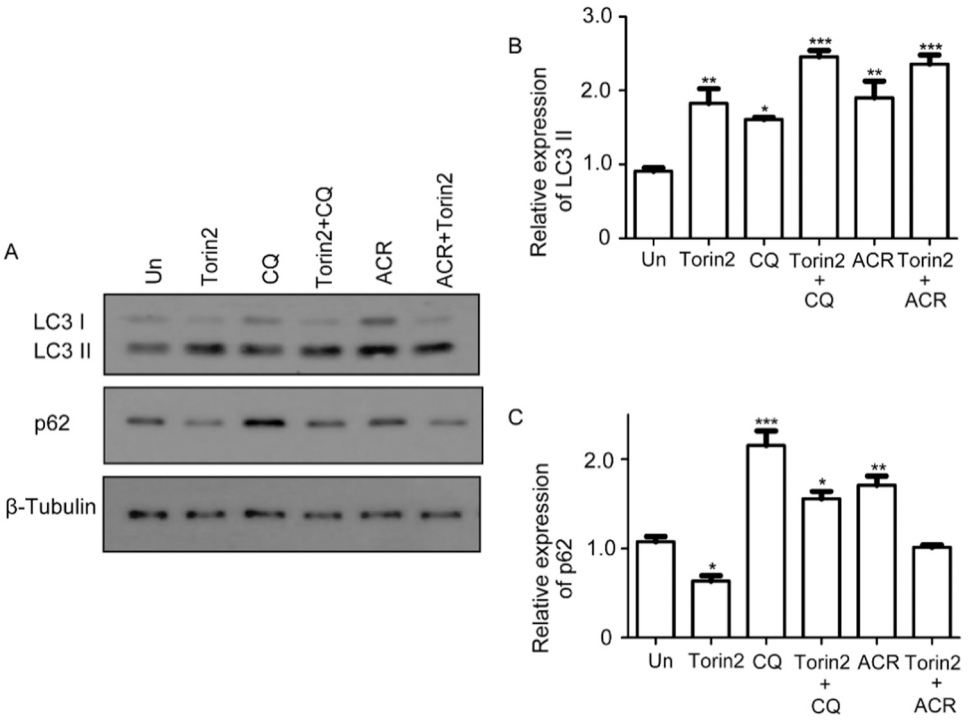

Fig. 3. ACR blocks autophagosome maturation. (A) U_2OS cells were incubated with autophagy activator Torin2, lysosome inhibitor chloroquine (CQ), Torin2 plus CQ, or 1 μM ACR with/without Torin2 for 6 h. LC3-II and p62 levels were analyzed by western blotting. (B, C) Quantification of relative LC3-II and p62 levels were from three independent experiments as in A. Data are shown as the mean ± SEM and analyzed by Student's *t*-test. $^{*}P < 0.05$, $^{**}P < 0.01$, $^{***}P < 0.001$. Un: Untreated controls.

found that ACR treatment elevated the p62 level. LC3-II levels were further accumulated upon Torin2 plus ACR treatment when compared with ACR alone. Overall, these results suggest that ACR blocks autophagic flux, and this effect is comparable with that of CQ.

3.4. ACR induces ROS accumulation, cell apoptosis and inflammation

Our previous study have showed that the blocked autophagy flux could cause ROS accumulation (Song et al., 2019a). Thus, we detected the ROS levels by conversion of DCFH-DA to the fluorescent dye 2′,7′-dichlorofluorescein (Fig. 4A, B). This result showed that ACR significantly increased ROS production. Moreover, ROS generation can induce apoptosis and even necrosis (Wang et al., 2015). Flow cytometry results indicated that the rate of apoptosis (Q2 + Q3) was increased under ACR treatment (Fig. 4C). Similarly, our quantitative real-time PCR results showed that ACR significantly increased the mRNA levels of the pro-apoptosis genes Bax (a pro-apoptotic member of the Bcl-2 (β-cell lymphoma-2) protein family), and Caspase3 and Caspase8 (Caspases are

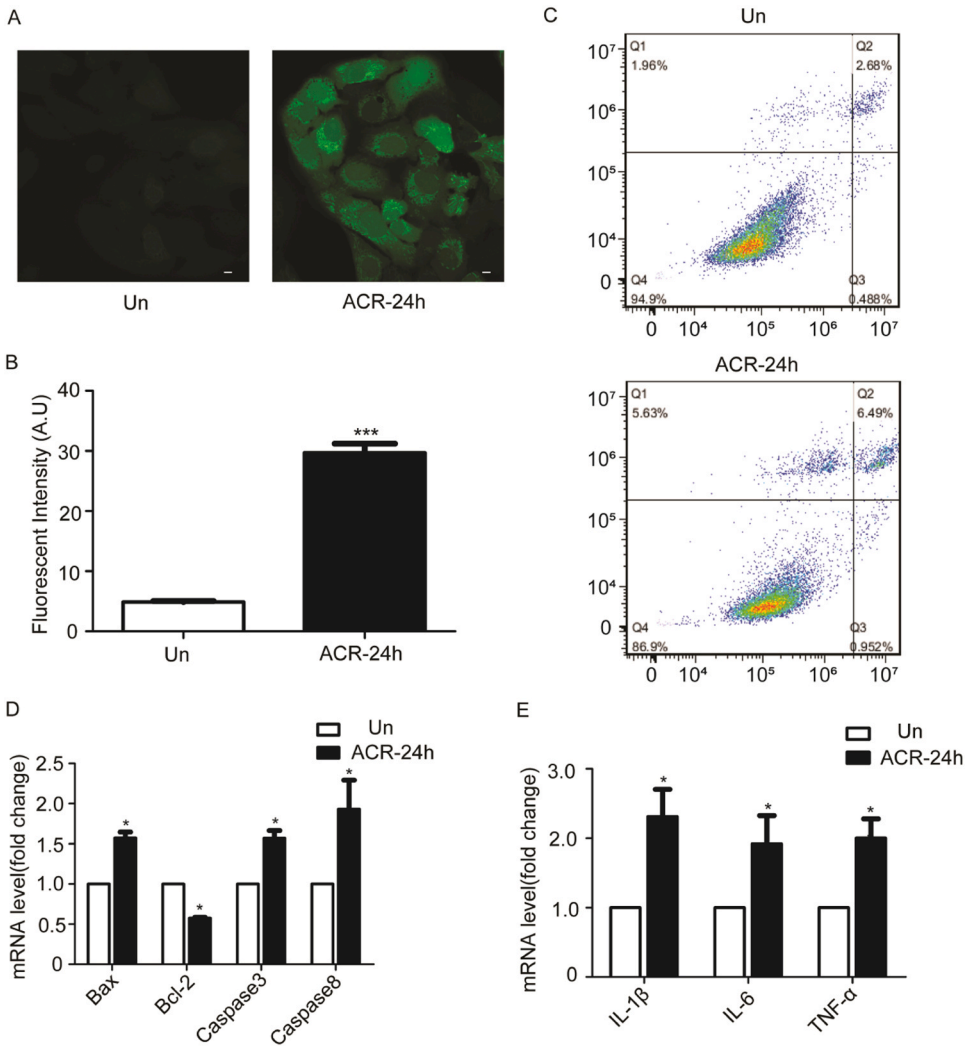

Fig. 4. ACR increases ROS content, induces cell apoptosis and inflammation generation. (A) ROS was detected by immunofluorescence by conversion of DCFH-DA to the fluorescent dye 2′,7′-dichlorofluorescein. (B) Quantification of ROS fluorescent intensity, analyzed by Student's *t*-test. (C) Apoptosis analysis by flow cytometry after ACR treatment. (D) mRNA levels of pro and anti apoptosis-related genes in U_2OS cells. Bax: a pro-apoptotic member of the Bcl-2 (β-cell lymphoma-2) protein family, Caspase3 and Caspase8: Proteinases involved in activation of apoptosis, Bcl-2, an inhibitor of the actions of pro-apoptotic proteins. (E) mRNA levels of inflammation-related genes including interleukin-1β (IL-1β), interleukin-6 (IL-6) and tumor necrosis factor α (TNF-α) in U_2OS cells. Data are shown as the mean ± SEM and analyzed by Student's *t*-test. Un: untreated controls.

cysteine-aspartic acid proteinases involved in activation of apoptosis) and reduced Bcl-2 (anti-apoptosis gene) mRNA expression level (Fig. 4D). In addition, we observed that the transcription levels of the inflammation-related genes interleukin-1β, interleukin-6 and tumor necrosis factor α were significantly upregulated by ACR treatment (Fig. 4E). Together these results suggest that ACR could increase ROS content, induce cell apoptosis and inflammation generation.

3.5. Metabolomic profiles analysis

Multivariate statistical analyses were performed to compare the differences in the metabolomes between the ACR-treated group and control group. Firstly, the PCA score plots of quality control (QC) samples were analyzed to evaluate the stability and repeatability of the high-performance liquid chromatography-tandem mass spectrometry (HPLC-MS/MS) system. We noted that the PCA analysis of QC samples showed a tight cluster and there was a clear separation between other groups and no overlap, indicating that HPLC-MS/MS system has a high stability (Fig. S1A). Subsequently, we conducted a PCA model analysis to compare the discrete differences between the ACR treated group and the control group. As shown in Fig. S1B, the PCA score plots exhibited distinct separation between the different groups (the sum of PC1and PC2 explained 61.9% of the total variation). Thereafter, PLS-DA was performed to further validate the difference. Similarly, as shown in Fig. S1C, an obvious separation was observed on PLS-DA score plot between ACR and control groups ($R^2 = 0.995$, $Q^2 = 0.829$). In addition, 200 permutation tests were performed on the model parameters to verify the reliability of PLS-DA model (Fig. S1D). R^2-intercepts and Q^2-intercepts were 0.919 and − 0.00157, and all Q^2 were lower than R^2, which means that the PLS-DA model was not overfitting and effective. Overall, these results indicate that there is a significant difference in the metabolic profiles of ACR treated and control groups.

Based on the PLS-DA analysis, variable importance in the projection (VIP > 1 and $P < 0.05$) was used to screen for the main metabolic markers of the two groups. Here, we identified 73 key metabolites whose levels were influenced by the ACR treatment (Table S2). Specifically, a total of 29 and 24 differential metabolites were identified in the positive and negative ion modes, respectively, and 20 differential metabolites were identified by TSQ Quantiva. These identified metabolites included carbohydrates, lipids, amino acids, organic acids, and other types of compounds. Among the 73 different key metabolites, 16 were significantly decreased, and 57 were significantly elevated under ACR treatment. In order to make differences more visible in the two groups, a heat map was generated by MetaboAnalyst 3.0 (Fig. 5). The abscissa represents different treatment groups, the ordinate represents the differential metabolites of each group, and the red color represents an increase in metabolites in ACR treated groups when compared with control, green color represents a decrease. It was apparent that most of differential metabolites were up-regulated after ACR treatment.

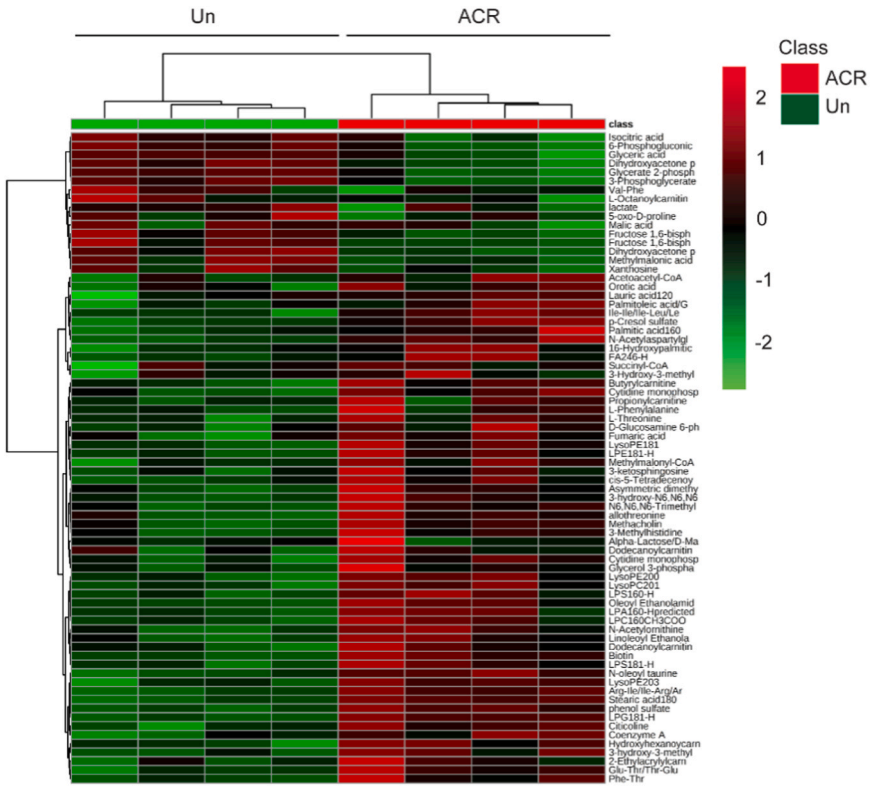

Fig. 5. Hierarchical clustering analysis of differential metabolites between ACR treated and control groups in U_2OS cells. The rows and columns represent differential metabolites and experimental samples, respectively. Red boxes show up-regulated metabolites and green boxes show down-regulated metabolites under ACR treatment. The scale indicates fold change. (For interpretation of the references to colour in this figure legend, the reader is referred to the web version of this article.)

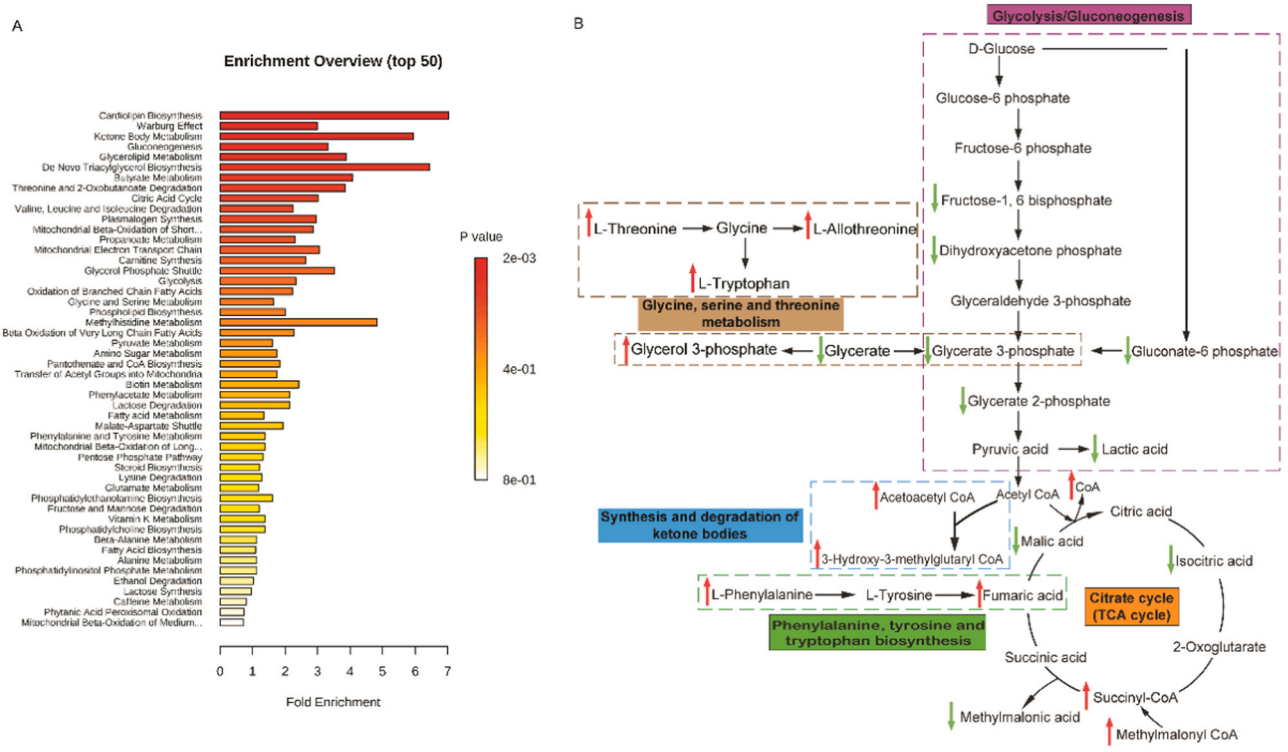

Fig. 6. ACR alters multiple metabolic pathways. (A) Enriched metabolic pathway analysis after ACR treatment of U_2OS cells. (B) Schematic diagram of major differential metabolic pathways after ACR treatment in U_2OS cells. Red arrows represent up-regulated metabolites, green arrows represent down-regulated metabolites. (For interpretation of the references to colour in this figure legend, the reader is referred to the web version of this article.)

3.6. Metabolic pathway analysis

Metabolic pathway enrichment was generated based on the KEGG pathway database by MetaboAnalyst 3.0. As shown in Fig. 6A, many metabolic pathways were identified on the basis of the enrichment fold of pathways analysis, the major altered pathways in the top ten included cardiolipin biosynthesis, the Warburg effect, ketone body metabolism, gluconeogenesis, glycerolipid metabolism, De Novo triacylglycerol biosynthesis, butyrate metabolism, threonine and 2-Oxobutanoate degradation, citric acid cycle, valine, leucine and isoleucine degradation. A detailed description of the major altered pathways was shown in Table S3. A metabolic network map is displayed in Fig. 6B. The red arrows indicate a higher level, while the green arrows indicate a lower level in the ACR treated group. The relative content of glycolytic and TCA cycle intermediates in ACR group were significantly lower than those of the control group, while the relative contents of some of the amino acids detected in ACR group were significantly higher. Overall, this metabolic network shows a more intuitive correlation between the identified differential metabolites.

4. Discussion

In the present study, we investigated the metabolic profiling of ACR treatment using HPLC-MS based metabolomics combined with multivariate data analysis. We observed that exposure to ACR exhibited distinct differences in metabolic profiles from PCA, PLS-DA and hierarchical clustering analyses in comparison with controls. A total of 73 differential metabolites were identified, and they showed a tight correlation in several pathways, including glycolysis, tricarboxylic acid (TCA) cycle, amino acids metabolism, and lipids metabolism and so on. This result was similar to previous proteomics results, which revealed that ACR induced protein changes in the TCA cycle and glycolysis pathways (Nagashima et al., 2019).

Changes in the glycolysis/gluconeogenesis were found in the current study. Several of glycolytic intermediates were decreased after ACR treatment, such as levels of fructose-1,6 diphosphate, dihydroxyacetone phosphate, glycerate 3-phosphate, gluconate-6 phosphate, glycerate 2-phosphate, and lactic acid. Glycolysis provides substrate for the TCA cycle in most of organisms (Birungi et al., 2010; Schormann et al., 2019). Decreased glycolysis intermediates indicated that the metabolic rate of glycolysis was significantly slowed down, which may also be one of the causes for attenuated carbon flow rate of the TCA cycle.

The TCA cycle is an epicenter in cell metabolism pathway because it participates in both anabolism and catabolism. It is the ultimate common pathway of amino acid, fatty acid, and carbohydrate metabolism, and is the most important metabolic pathway for the body's energy supply (Akram, 2014). In this study, several TCA intermediates (isocitric acid, malic acid as well as methylmalonic acid) levels were significantly reduced in the ACR treated group. The decreases in TCA intermediates levels imply a restricted TCA cycle, mitochondrial respiratory defect, and energy deficiency (Araújo et al., 2018; Ma et al., 2013). Several studies have suggested that exposure to ACR attenuates the activity of the mitochondrial electron transfer chain complex, indicating increased oxidative stress (Kumar and K, 2019; Zamani et al., 2017). Zhao et al. (2015) have confirmed that ACR-induced neurotoxicity and genotoxicity were associated with the changes in oxidative status and mitochondrial function. They proved that exposure to ACR induced overproduction of ROS levels, increased mitochondrial membrane permeability and reduced activities of ATPase as well as superoxide dismutase. This is consistent with our results, where we observed that ACR treatment significantly increased ROS levels. Although a higher fumaric acid level was detected, this is probably due to the increase in the level of L-phenylalanine, because it can be converted into tyrosine, and then further metabolized into fumaric acid, and then enter the TCA cycle. Tang et al. (2019) verified that the accumulated fumaric acid contributed to increased ROS production, which is associated with the attenuated TCA cycle. Together, our data suggests that exposure to ACR increase fumaric acid levels and induces ROS accumulation, thereby attenuating TCA cycle rate.

Lipids and their derivatives are important cellular membrane structures, and play critical roles in regulating multiple signal transduction pathways, such as cell proliferation, apoptosis, and membrane trafficking (Bou Khalil et al., 2010). Among the detected lipids, lysophosphatidic acid (LPA), lysophosphatidylcholine (LPC), lysophosphatidylserine (LPS), and lysophosphatidylglycerol (LPG) levels showed a significant increase under ACR treatment. It has been shown that high levels of LPA may induce neuronal cell apoptosis and necrosis in a rat model (Steiner et al., 2000). LPC acts as an important inflammatory mediator and could induce expression of inflammatory proteins and mitochondrial ROS generation, thereby impairing mitochondrial function (Li et al., 2016b; Tseng et al., 2019). Thus, the increased lipid metabolites implied that exposure to ACR may promote ROS accumulation and cell apoptosis, our results are fully consistent with this point of view. Moreover, the impaired autolysosome maturation was associated with elevated lipid content (Song et al., 2019b). In this study, our results showed that exposure to ACR significantly upregulated autophagy protein (LC3-II and p62) levels, and blocked the degradation process, thereby inhibiting autophagy, which may prevent the degradation and renewal of lipids. This is the first research to elucidate the underlying effect of ACR on autophagy. In addition, studies have shown that ROS acts as cell signaling molecules to initiate the formation and degradation of autophagosomes (Azad et al., 2009; Chen et al., 2009). In contrast, oxidative damage and ROS levels could be reduced by autophagy removing damaged organelles such as protein aggregates and mitochondria (Scherz-Shouval and Elazar, 2007; Signorelli et al., 2019). Therefore, we suspected that the blocked autophagic flux may also be one of the reasons for the ROS levels accumulation.

Amino acids act as signals regulating the cell growth and development, and metabolic pathways (Herring et al., 2018). We noted that several of the identified amino acids were significantly accumulated under ACR treatment. Among them, 3-methylhistidine is identified as a biomarker of skeletal muscle toxicity (Aranibar et al., 2011). Asymmetric dimethylarginine accumulation increased chronic kidney disease risk (Liu et al., 2018). It has been reported that L-threonine supplementation could alleviate the inflammatory responses in the intestine of lipopolysaccharide-induced broilers (Chen et al., 2018). Thus, in our results, the increased L-threonine may exert a compensatory effect to counter ACR-induced inflammation reaction. Also, there is evidence that amino acids are produced by autophagy degrading proteins in some cases (Ezaki et al., 2011). Excessive amino acids also might reduce autophagy levels (Yabu et al., 2012). Thus, one might speculate that the blocked autophagy flux is related to the increase of amino acid levels, and these increased amino acids levels may also be a risk factor for some diseases.

In this study, we determined the underlying effects of ACR on autophagy. Significant accumulation of LC3-II and p62 levels suggests that ACR inhibits autophagy via blocking autophagic flux. Metabolomics results suggested exposure to ACR restricted the rate of glycolysis and TCA cycle metabolism, and conversely, accelerated amino acid as well as fatty acid metabolism. Moreover, ACR caused ROS accumulation, induced cell apoptosis and inflammation.

Author contributions

D.S and C.X performed the biological and biochemical experiments. A. H. and R.L. conceived the project, designed the experiments, analyzed the data and wrote the manuscript with the help of all authors.

Declaration of Competing Interest

The authors declare that they have no known competing financial interests or personal relationships that could have appeared to influence the work reported in this paper.

Acknowledgements

The work was supported by grants to Rong Liu from the National Key Research and Development Program of China (Grant No. 2017YFD0400200), the Jiangsu Natural Science Funds for Distinguished Young Scholar (Grant no. BK20170025), the National Natural Science Foundation of China (Grant No. 31771532), the “Shuangchuang”, “Six talent peaks” and "333" projects in Jiangsu province.

Disclosure statement

The authors declare that there is no competing interest among them.

Appendix A. Supporting information

Supplementary data associated with this article can be found in the online version at doi:10.1016/j.ecoenv.2020.111543.

References

Akram, M., 2014. Citric acid cycle and role of its intermediates in metabolism. Cell Biochem. Biophys. 68, 475–478.
Aranibar, N., Vassallo, J.D., Rathmacher, J., Stryker, S., Zhang, Y., Dai, J., Janovitz, E.B., Robertson, D., Reily, M., Lowe-Krentz, L., Lehman-McKeeman, L., 2011. Identification of 1- and 3-methylhistidine as biomarkers of skeletal muscle toxicity by nuclear magnetic resonance-based metabolic profiling. Anal. Biochem. 410, 84–91.
Araújo, A.M., Bastos, M.L., Fernandes, E., Carvalho, F., Carvalho, M., Guedes de Pinho, P., 2018. GC-MS metabolomics reveals disturbed metabolic pathways in primary mouse hepatocytes exposed to subtoxic levels of 3,4-methylenedioxymethamphetamine (MDMA). Arch. Toxicol. 92, 3307–3323.
Azad, M.B., Chen, Y., Gibson, S.B., 2009. Regulation of autophagy by reactive oxygen species (ROS): implications for cancer progression and treatment. Antioxid. Redox Signal. 11, 777–790.
Birungi, G., Chen, S.M., Loy, B.P., Ng, M.L., Li, S.F.Y., 2010. Metabolomics approach for investigation of effects of dengue virus infection using the EA.hy926 cell line. J. Proteome Res. 9, 6523–6534.
Bou Khalil, M., Hou, W., Zhou, H., Elisma, F., Swayne, L.A., Blanchard, A.P., Yao, Z., Bennett, S.A.L., Figeys, D., 2010. Lipidomics era: accomplishments and challenges. Mass Spectrom. Rev. 29, 877–929.
Cheng, J., Zhang, S., Wang, S., Wang, P., Su, X.O., Xie, J., 2019. Rapid and sensitive detection of acrylamide in fried food using dispersive solid-phase extraction combined with surface-enhanced Raman spectroscopy. Food Chem. 276, 157–163.
Chen, Y., Azad, M.B., Gibson, S.B., 2009. Superoxide is the major reactive oxygen species regulating autophagy. Cell Death Differ. 16, 1040–1052.
Chen, Y., Zhang, H., Cheng, Y., Li, Y., Wen, C., Zhou, Y., 2018. Dietary l-threonine supplementation attenuates lipopolysaccharide-induced inflammatory responses and intestinal barrier damage of broiler chickens at an early age. Br. J. Nutr. 119, 1254–1262.
Daniali, G., Jinap, S., Sanny, M., Tan, C.P., 2018. Effect of amino acids and frequency of reuse frying oils at different temperature on acrylamide formation in palm olein and soy bean oils via modeling system. Food Chem. 245, 1–6.
Delbridge, L.M.D., Mellor, K.M., Taylor, D.J., Gottlieb, R.A., 2017. Myocardial stress and autophagy: mechanisms and potential therapies. Nat. Rev. Cardiol. 14, 412–425.
Exon, J.H., 2006. A review of the toxicology of acrylamide. J. Toxicol. Environ. Health B Crit. Rev. 9, 397–412.
Ezaki, J., Matsumoto, N., Takeda-Ezaki, M., Komatsu, M., Takahashi, K., Hiraoka, Y., Taka, H., Fujimura, T., Takehana, K., Yoshida, M., Iwata, J., Tanida, I., Furuya, N., Zheng, D.M., Tada, N., Tanaka, K., Kominami, E., Ueno, T., 2011. Liver autophagy contributes to the maintenance of blood glucose and amino acid levels. Autophagy 7, 727–736.
Friedman, M., 2003. Chemistry, biochemistry, and safety of acrylamide. A review. J. Agric. Food Chem. 51, 4504–4526.
Galluzzi, L., Baehrecke, E.H., Ballabio, A., Boya, P., Bravo-San Pedro, J.M., Cecconi, F., Choi, A.M., Chu, C.T., Codogno, P., Colombo, M.I., Cuervo, A.M., Debnath, J., Deretic, V., Dikic, I., Eskelinen, E.L., Fimia, G.M., Fulda, S., Gewirtz, D.A., Green, D. R., Hansen, M., Harper, J.W., Jäättelä, M., Johansen, T., Juhasz, G., Kimmelman, A. C., Kraft, C., Ktistakis, N.T., Kumar, S., Levine, B., Lopez-Otin, C., Madeo, F., Martens, S., Martinez, J., Melendez, A., Mizushima, N., Münz, C., Murphy, L.O., Penninger, J.M., Piacentini, M., Reggiori, F., Rubinsztein, D.C., Ryan, K.M., Santambrogio, L., Scorrano, L., Simon, A.K., Simon, H.U., Simonsen, A., Tavernarakis, N., Tooze, S.A., Yoshimori, T., Yuan, J., Yue, Z., Zhong, Q., Kroemer, G., 2017. Molecular definitions of autophagy and related processes. EMBO J. 36, 1811–1836.
Herring, C.M., Bazer, F.W., Johnson, G.A., Wu, G., 2018. Impacts of maternal dietary protein intake on fetal survival, growth, and development. Exp. Biol. Med. (Maywood) 243, 525–533.
Hsu, P., Shi, Y., 2017. Regulation of autophagy by mitochondrial phospholipids in health and diseases. Biochim Biophys. Acta Mol. Cell Biol. Lipids 1862, 114–129.
Kacar, S., Sahinturk, V., Kutlu, H.M., 2019. Effect of acrylamide on BEAS-2B normal human lung cells: cytotoxic, oxidative, apoptotic and morphometric analysis. Acta Histochem. 121, 595–603.
Krishnan, M., Kang, S.C., 2019. Vitexin inhibits acrylamide-induced neuroinflammation and improves behavioral changes in zebrafish larvae. Neurotoxicol. Teratol. 74, 106811.
Kumar, P.P., K, V.H., 2019. Low Molecular Weight Chitosan (approximately 20 kDa) protects acrylamide induced oxidative stress in D. melanogaster by restoring dopamine and KIF5B levels. Carbohydr. Polym. 222, 115005.
Liu, Z., Song, G., Zou, C., Liu, G., Wu, W., Yuan, T., Liu, X., 2015. Acrylamide induces mitochondrial dysfunction and apoptosis in BV-2 microglial cells. Free Radic. Biol. Med. 84, 42–53.
Liu, X., Xu, X., Shang, R., Chen, Y., 2018. Asymmetric dimethylarginine (ADMA) as an important risk factor for the increased cardiovascular diseases and heart failure in chronic kidney disease. Nitric Oxide Biol. Chem. 78, 113–120.
Li, T., Cao, J., Li, Z., Wang, X., He, P., 2016a. Broad screening and identification of beta-agonists in feed and animal body fluid and tissues using ultra-high performance liquid chromatography-quadrupole-orbitrap high resolution mass spectrometry combined with spectra library search. Food Chem. 192, 188–196.
Li, X., Fang, P., Li, Y., Kuo, Y.M., Andrews, A.J., Nanayakkara, G., Johnson, C., Fu, H., Shan, H., Du, F., Hoffman, N.E., Yu, D., Eguchi, S., Madesh, M., Koch, W.J., Sun, J., Jiang, X., Wang, H., Yang, X., 2016b. Mitochondrial reactive oxygen species mediate lysophosphatidylcholine-induced endothelial cell activation. Arterioscler. Thromb. Vasc. Biol. 36, 1090–1100.
LoPachin, R.M., Balaban, C.D., Ross, J.F., 2003. Acrylamide axonopathy revisited. Toxicol. Appl. Pharmacol. 188, 135–153.
Ma, B., Li, X., Zhang, Q., Wu, D., Wang, G., A, J., Sun, J., Li, J., Liu, Y., Wang, Y., Ying, H., 2013. Metabonomic profiling in studying anti-osteoporosis effects of strontium fructose 1,6-diphosphate on estrogen deficiency-induced osteoporosis in rats by GC/TOF-MS. Eur. J. Pharmacol. 718, 524–532.
Mizushima, N., Levine, B., 2010. Autophagy in mammalian development and differentiation. Nat. Cell Biol. 12, 823–830.
Nagashima, D., Zhang, L., Kitamura, Y., Ichihara, S., Watanabe, E., Zong, C., Yamano, Y., Sakurai, T., Oikawa, S., Ichihara, G., 2019. Proteomic analysis of hippocampal proteins in acrylamide-exposed Wistar rats. Arch. Toxicol. 93, 1993–2006.
Scharer, O.D., 2003. Chemistry and biology of DNA repair. Angew. Chem. Int. Ed. 42, 2946–2974.
Scherz-Shouval, R., Elazar, Z., 2007. ROS, mitochondria and the regulation of autophagy. Trends Cell Biol. 17, 422–427.
Schormann, N., Hayden, K.L., Lee, P., Banerjee, S., Chattopadhyay, D., 2019. An overview of structure, function and regulation of Pyruvate Kinases. Protein Sci. 28, 1771–1784.
Shipp, A., Lawrence, G., Gentry, R., McDonald, T., Bartow, H., Bounds, J., Macdonald, N., Clewell, H., Allen, B., Van Landingham, C., 2006. Acrylamide: review of toxicity data and dose-response analyses for cancer and noncancer effects. Crit. Rev. Toxicol. 36, 481–608.
Signorelli, S., Tarkowski, Ł.P., Van den Ende, W., Bassham, D.C., 2019. Linking autophagy to abiotic and biotic stress responses. Trends Plant Sci. 24, 413–430.
Song, D., Chen, Y., Wang, B., Li, D., Xu, C., Huang, H., Huang, S., Liu, R., 2019a. Bisphenol A inhibits autophagosome-lysosome fusion and lipid droplet degradation. Ecotoxicol. Environ. Saf. 183, 109492.
Song, D., Guo, R., Huang, H., Zheng, P., Huang, H., Oyang, Q., Xiao, X., Wang, B., Rong, J., Liu, R., 2019b. 2-Amino-3,8-dimethylimidazo[4,5-f]quinoxaline alters autophagosome maturation, cellular lipidomic profiles, and expression of core pluripotent factors. J. Agric. Food Chem. 67, 7977–7985.
Song, G., Liu, Z., Wang, L., Shi, R., Chu, C., Xiang, M., Tian, Q., Liu, X., 2017. Protective effects of lipoic acid against acrylamide-induced neurotoxicity: involvement of mitochondrial energy metabolism and autophagy. Food Funct. 8, 4657–4667.
Steiner, M.R., HOLTSBERG, F.W., KELLER, J.N., MATTSON, M.P., STEINER, S.M., 2000. Lysophosphatidic acid induction of neuronal apoptosis and necrosis. Ann. N. Y. Acad. Sci. 905, 132–141.
Sumner, S.C.J., 2003. Acrylamide: a comparison of metabolism and hemoglobin adducts in rodents following dermal, intraperitoneal, oral, or inhalation exposure. Toxicol. Sci. 75, 260–270.
Taira, T., et al., 2004. DJ-1 has a role in antioxidative stress to prevent cell death (vol 5, pg 213, 2004). Embo Reports. 5, 430–430.
Tai, Y., Wei, C., Yang, H., Zhang, L., Chen, Q., Deng, W., Wei, S., Zhang, J., Fang, C., Ho, C., Wan, X., 2015. Transcriptomic and phytochemical analysis of the biosynthesis of characteristic constituents in tea (Camellia sinensis) compared with oil tea (Camellia oleifera). BMC Plant Biol. 15, 190.

Tan, X., et al., 2018. Acrylamide aggravates cognitive deficits at night period via the gut-brain axis by reprogramming the brain circadian clock. Arch. Toxicol.
Tang, K., Yu, Y., Zhu, L., Xu, P., Chen, J., Ma, J., Zhang, H., Fang, H., Sun, W., Zhou, L., Wei, K., Li, F., Lv, J., Xie, J., Liu, Y., Huang, B., 2019. Hypoxia-reprogrammed tricarboxylic acid cycle promotes the growth of human breast tumorigenic cells. Oncogene 38, 6970–6984.
Tseng, H.C., Lin, C.C., Hsiao, L.D., Yang, C.M., 2019. Lysophosphatidylcholine-induced mitochondrial fission contributes to collagen production in human cardiac fibroblasts. J. Lipid Res. 60, 1573–1589.
Vainio, H., Heseltine, E., Wilbourn, J., 1994. Priorities for future IARC monographs on the evaluation of carcinogenic risks to humans. Environ. Health Perspect. 102, 590–591.
Wang, R., Lu, L., Guo, Y., Lin, F., Chen, H., Chen, W., Chen, M., 2015. Effect of glucagon-like Peptide-1 on high-glucose-induced oxidative stress and cell apoptosis in human endothelial cells and its underlying mechanism. J. Cardiovasc. Pharmacol. 66, 135–140.
Yabu, T., Imamura, S., Mizusawa, N., Touhata, K., Yamashita, M., 2012. Induction of autophagy by amino acid starvation in fish cells. Mar. Biotechnol. 14, 491–501.
Zamani, E., Shaki, F., AbedianKenari, S., Shokrzadeh, M., 2017. Acrylamide induces immunotoxicity through reactive oxygen species production and caspase-dependent apoptosis in mice splenocytes via the mitochondria-dependent signaling pathways. Biomed. Pharm. 94, 523–530.
Zhang, W., Huai, W., Zhang, Y., Shen, J., Tang, X., Xie, X., Wang, K., Fan, H., 2017. Ultra-performance liquid chromatography hyphenated with quadrupole-orbitrap mass spectrometry for simultaneous determination of necine-core-structure pyrrolizidine alkaloids in Crotalaria sessiliflora L. without all corresponding standards. Phytochem. Anal. 28, 365–373.
Zhao, M., Wang, P., Zhu, Y., Liu, X., Hu, X., Chen, F., 2015. The chemoprotection of a blueberry anthocyanin extract against the acrylamide-induced oxidative stress in mitochondria: unequivocal evidence in mice liver. Food Funct. 6, 3006–3012.